

Variations in soil carbonate formation and seasonal bias over >4 km of relief in the western Andes (30°S) revealed by clumped isotope thermometry



Landon Burgener ^{a,*}, Katharine W. Huntington ^a, Gregory D. Hoke ^b, Andrew Schauer ^a, Mallory C. Ringham ^a, Claudio Latorre ^{c,d}, Francisca P. Díaz ^e

^a Department of Earth and Space Sciences, University of Washington, Seattle, WA, United States

^b Department of Earth Sciences, Syracuse University, Syracuse, NY, United States

^c Departamento de Ecología, Pontificia Universidad Católica de Chile, Santiago, Chile

^d Institute of Ecology and Biodiversity, Santiago, Chile

^e Departamento de Microbiología y Genética Molecular, Pontificia Universidad Católica de Chile, Santiago, Chile

ARTICLE INFO

Article history:

Received 21 September 2015

Received in revised form 10 February 2016

Accepted 16 February 2016

Available online 3 March 2016

Editor: H. Stoll

Keywords:

pedogenic carbonate
clumped isotopes
soil moisture
soil carbonate formation
cryogenic carbonates
kinetic isotope effects

ABSTRACT

Carbonate clumped isotope thermometry provides a new method for investigating long-standing questions regarding seasonal biases in soil carbonate formation and the relationship between soil carbonate formation temperatures recorded by clumped isotopes ($T(\Delta_{47})$) and surface temperatures. We address these questions by comparing C, O, and clumped isotope data from Holocene soil carbonates to meteorological and in situ soil monitoring data along a 170 km transect with >4 km of relief in Chile (30°S). This arid transect experiences a winter wet season, and a >20°C range in mean annual air temperature. We test the hypothesis that, regardless of soil moisture conditions, soil carbonates from arid regions record warm season biases and form in isotopic equilibrium with soil water and soil CO₂. Below 3200 m, precipitation falls as rain and soil carbonate $T(\Delta_{47})$ values at depths >40 cm resemble summer soil temperatures. Above 3200 m, precipitation falls as snow and $T(\Delta_{47})$ values resemble mean annual soil temperatures. Soil carbonates from the highest site yield anomalous $\delta^{18}\text{O}$, $\delta^{13}\text{C}$, and $T(\Delta_{47})$ values indicative of kinetic isotope effects consistent with cryogenic carbonate formation. Our findings (1) demonstrate that soil carbonate $T(\Delta_{47})$ values from shallow (<40 cm) depths can be affected by short-term temperature changes following precipitation events; (2) suggest that only the largest precipitation events affect soil moisture at depths >40 cm; (3) highlight the role of the soil moisture regime in modulating the timing of soil carbonate formation, which affects the resulting carbonate $T(\Delta_{47})$ values; and (4) show that soil carbonates from high elevation or high latitude sites may form under non-equilibrium conditions. These findings underscore the importance of understanding past soil moisture conditions when attempting to reconstruct paleotemperatures using carbonate clumped isotope thermometry.

© 2016 Elsevier B.V. All rights reserved.

1. Introduction

The application of the carbonate clumped-isotope paleothermometer to pedogenic (formed in soil) carbonates has shed new light on a variety of paleoclimate and tectonic questions (Eagle et al., 2013; Garzione et al., 2008, 2014; Ghosh et al., 2006a; Leier et al., 2013; Passey et al., 2010; Quade et al., 2007a, 2007b, 2011; Snell et al., 2013, 2014; Suarez et al., 2011). Studies of modern soil carbonates provide context for paleoproxy interpretations by inves-

tigating the relationship between soil carbonate clumped isotope temperatures (hereafter $T(\Delta_{47})$) and the environmental conditions under which the carbonates formed (e.g., Hough et al., 2014; Passey et al., 2010; Peters et al., 2013; Quade et al., 2013). However, full utilization of soil carbonates as paleotemperature proxies has been hampered by several unresolved questions: (1) When does soil carbonate form? (2) How do soil carbonate formation temperatures relate to surface temperatures? (3) Are $T(\Delta_{47})$ values of soil carbonates from different environments (e.g., tropical versus high latitude) directly comparable? With regard to the first two questions, several studies (e.g., Breecker et al., 2009; Passey et al., 2010; Quade et al., 2013) suggest that carbonate formation is biased towards summer soil drying events, and that

DOI of related article: <http://dx.doi.org/10.1016/j.epsl.2016.02.003>.

* Corresponding author.

E-mail address: lkb57@uw.edu (L. Burgener).

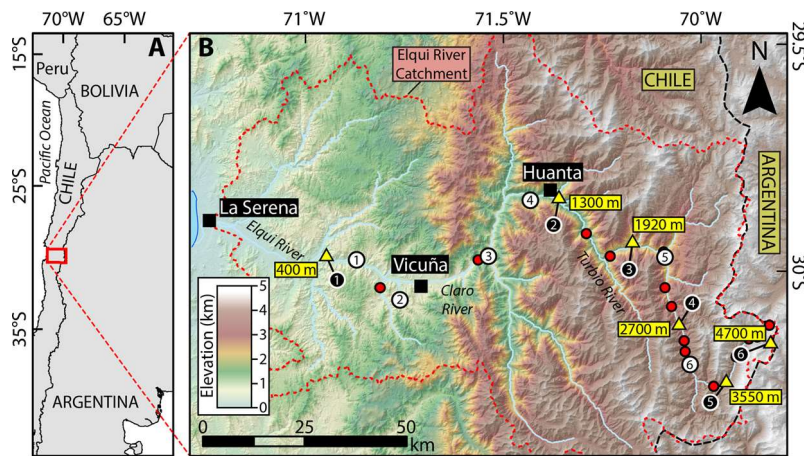


Fig. 1. (A) Shaded relief map showing the location of the 1 m soil pits (yellow triangles), single 50 cm samples (red circles), weather stations maintained by the Chilean government (numbered white circles), and the weather stations installed for this study (numbered black circles). The upper regions of the Elqui River catchment (red dashed line) lie along the Chile–Argentina border (black dashed line). (B) Map shows the location of the study area.

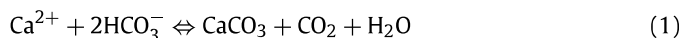
$T(\Delta_{47})$ values show a warm-season bias regardless of soil moisture conditions (Quade et al., 2013); however, some soil carbonates form under differing seasonal biases due to change in soil moisture (Peters et al., 2013), or under non-equilibrium conditions (e.g., Courty et al., 1994; Tabor et al., 2013), suggesting that comparing soil carbonates from different environments or determining the seasonal bias of ancient soil carbonates may not be a straightforward exercise.

We address these questions by collecting Holocene soil carbonates over >4 km of topographic relief on the western flank of the Andes, in north-central Chile (30°S). The range in environmental conditions along this transect allows us to investigate how soil carbonate $\delta^{18}\text{O}$, $\delta^{13}\text{C}$, and $T(\Delta_{47})$ values record environmental conditions under changing soil moisture and temperature regimes. At sites below the winter snow line carbonate $\delta^{18}\text{O}$, $\delta^{13}\text{C}$, and $T(\Delta_{47})$ values are consistent with a warm season bias in carbonate formation. Carbonates from above the snow line yield $T(\Delta_{47})$ values similar to mean annual soil temperature (MAST). Our findings are consistent with the hypothesis that in hot arid environments, a warm-season bias in $T(\Delta_{47})$ values predominates, but that significant changes in soil moisture conditions (e.g., effect of spring snowmelt on the timing of soil drying) can impact soil carbonate $T(\Delta_{47})$ values. Additionally, we show that in high elevation or extremely arid climates, non-equilibrium processes can lead to anomalous $\delta^{18}\text{O}$, $\delta^{13}\text{C}$, and $T(\Delta_{47})$ values that do not reflect local climate.

2. Background

2.1. Soil carbonate formation and isotopic composition

Pedogenic carbonates (CaCO_3) are common in arid to subhumid environments (Landi et al., 2003). Carbonate precipitation follows the reaction:



Calcium ions are introduced into the soil water solution via deposition of dust, dissolution of minerals, and rainwater infiltration (Gile et al., 1966; Machette, 1985; Monger and Wilding, 2006). Carbon is supplied by respiration (vegetation and microbes) and atmospheric CO_2 , and oxygen is derived from soil waters (e.g., Cerling and Quade, 1993). Precipitation and dissolution of soil carbonates are influenced by soil conditions, including temperature, moisture and $p\text{CO}_2$ (e.g., Breecker et al., 2009; Drever, 1988; Stern et al., 1999). Carbonate formation occurs when the soil solution becomes

supersaturated in calcite due to dewatering, CO_2 outgassing, or an increase in Ca^{2+} or HCO_3^- in the solution (Breecker et al., 2009; Retallack, 2005).

Due to the slow rate of change in soil $p\text{CO}_2$ and temperature, carbonates are assumed to form in isotopic equilibrium with soil CO_2 and water (Cerling and Quade, 1993). The isotopic composition of soil carbonates therefore acts as a time-integrated record of local environmental changes over hundreds to thousands of years. Soil carbonate $\delta^{18}\text{O}$ and $\delta^{13}\text{C}$ values reflect soil water isotopic compositions and soil productivity or vegetation type, respectively (Cerling and Quade, 1993; Meyer et al., 2014), whereas the clumped isotope (Δ_{47}) composition records soil temperature (Eiler, 2011; Peters et al., 2013; Quade et al., 2007a, 2007b, 2013).

Clumped-isotope thermometry provides a thermodynamics-based measurement of carbonate formation temperature (Eiler, 2007, 2011; Eiler et al., 2014; Ghosh et al., 2006b). Correlations between soil temperature data and soil carbonate $T(\Delta_{47})$ values suggest that the dewatering/outgassing events driving soil carbonate formation typically occur during the summer months, leading to a warm-season bias in $T(\Delta_{47})$ values (Hough et al., 2014; Passey et al., 2010; Peters et al., 2013; Quade et al., 2013; Suarez et al., 2011). However, it has been hypothesized that $T(\Delta_{47})$ values that do not reflect summer soil temperatures are the result of unique soil moisture balance conditions that change the seasonality of soil drying events (Peters et al., 2013).

2.2. The Elqui and Turbio valleys, Chile

The study area is situated in the Elqui River catchment of north-central Chile (Fig. 1). The Elqui River and its tributary the Turbio River have headwaters in the western flank of the Andes and outlet into the Pacific Ocean. The study area is divided into three geomorphic regions: 1) between 0 and ~750 m, the valley is a wide (500 m to 4 km) cultivated fluvial plain with alluvial fans prevalent near the valley walls; 2) between ~750 and 3200 m, the valley narrows (100 m to ~1 km) and is characterized by large debris fans and fluvial terraces; 3) above 3200 m, the valley widens and glacial landscapes dominate. We examine sites from 400 to >20 °C range in MAST.

Precipitation is controlled by the intensity and position of the South Pacific Subtropical High (Garreaud et al., 2009; Grosjean et al., 1998) and is characterized by a winter wet season and low mean annual precipitation (MAP) at all elevations (Fig. 2, Supplemental Fig. S1). The Dirección General de Aguas (DGA; <http://www.dga.cl/>) maintains meteorological stations (Fig. 1 and

Table 1

Weather stations maintained by the Dirección General de Aguas (DGA).

Station ^a	Station name	Lat (°N)	Lon (°E)	Elevation (m)	Data type
1	Almendral	−29.982	−70.919	370	Air T (1973–1989), Precip (1960–2014)
2	Vicuña	−30.057	−70.717	730	Precip (1971–2014)
3	Rivadavia	−29.977	−70.562	820	Air T (1972–2014), Precip (1960–2014)
4	Huanta	−29.848	−70.385	1240	Precip (1989–2014)
5	Las Juntas	−29.977	−70.094	2150	Air T (1990–2013), Precip (1990–2014)
6	La Laguna	−30.203	−70.042	3160	Air T (1974–2014), Precip (1964–2014)

^a Station number corresponds to the white numbered circles in Fig. 1.

Table 1) that provide daily precipitation data over much of the valley. From 1990 to 2014, MAP at elevations from 0 to 820 m averaged 90 mm yr^{−1}, and MAP at the Huanta (1240 m) and La Laguna (3160 m) stations averaged 60 mm yr^{−1} and 140 mm yr^{−1}, respectively. MAP at La Serena declined over the last century from 200 mm yr^{−1} in 1900 to 80 mm yr^{−1} in 2000 (Fiebig-Wittmaack et al., 2012), and DGA data show that the area experienced a 40% decrease in MAP between the 2000–2004 and 2005–2010 periods.

The large range in mean annual air temperatures (MAAT) along the transect (Fig. 2) results in rain at elevations <3200 m, and snow at higher elevations. Cool Pacific waters generate a thermal inversion resulting in a small surface temperature lapse rate between 0 and ∼2000 m. Above the thermal inversion (>2000 m) the surface temperature lapse rate is −6.2 °C km^{−1}. This pattern results in MAATs that decrease from ∼17 °C at 370 m (Station 1, Table 1) to 8 °C at 3160 m (Station 6). MAAT reaches subzero temperatures at ∼4500 m. Seasonal variations in air temperatures range from 7 °C on the coast to 13 °C at 3200 m. The large range in MAAT observed along the transect affects soil moisture balance, making it possible to compare the formation mechanisms affecting soil carbonates under a variety of temperature and soil moisture conditions.

3. Methods

3.1. Field methods

Surface water and carbonate samples were collected during January of 2013 and 2014. Water samples were collected from streams with flowing water with no evidence of flow contributed from upstream irrigation. All samples were collected in 15 ml centrifuge tubes with PTFE taped sealed threads and caps secured with electrical tape. Precipitation collectors consisting of 1 L HDPE Nalgene bottles fitted with ceramic Buchner funnels and filled with a 1–2 cm layer of oil were deployed at DGA-maintained meteorological stations. Any precipitated water that had accumulated in the bottle was collected on a monthly basis and the collector was redeployed after cleaning and adding fresh oil.

The 1 m soil pits were excavated at six elevations (Fig. 1), and sampled at ∼20 cm intervals beginning at 20 cm depth. Individual carbonate samples were collected at 50 cm depth from an additional fourteen sites (Fig. 1). At all elevations, soil development was weak to absent, with the substrate composed of conglomerates. We surveyed the main plant species present to within 100 m around each sample site and estimated the plant % cover. The plant species were identified based on a local vegetation catalogue (Marticorena et al., 2001). Below 3550 m, samples were collected from debris cone (∼11–5.5 ka) or fluvial terrace surfaces (5.5 ka); higher elevation samples were collected from a debris cone, terrace, or moraine surfaces (17–12 ka). The ages of glacial deposits in the Elqui/Turbo valleys were estimated from ¹⁰Be exposure ages of glacial features in the nearby Encierro Valley (Zech et al., 2006). The ages of debris cones and fluvial gravels in the Elqui valley were determined from radiocarbon ages on organic matter-rich layers (Riquelme et al., 2011). We targeted non-carbonate clasts bearing discontinuous

carbonate pendants, which Gile et al. (1966) identified as the initial form of carbonate growth in a rocky substrate. This allowed us to focus on Holocene and modern soil carbonates that should have integrated a limited number of climate fluctuations during their formation. To ensure the carbonate pendants had formed in situ, we only collected clasts with pendant formation on their underside. We note that most paleoclimate reconstructions make use of nodular carbonate collected from paleosols in sedimentary basins; however, mountainous regions with coarse-grained deposits are the only regions where we can explore such a large range of elevations over a short distance within a consistent moisture regime.

During the 2014 field season, meteorological stations were installed at each 1-m soil pit (Fig. 3). Onset data loggers (HOBO U30/NRC) were installed at monitoring sites at 400, 1300, 1900, 2700, and 3550 m. Soil temperature sensors (S-TMB-M006) were placed at depths of 10, 50, and 100 cm. One local soil moisture sensor (S-SMC-M005, 0.3 L volume of influence) was placed at 10 cm depth, and wide-area soil moisture sensors (S-SMD-M005, 1.0 L volume of influence) were placed at 50 and 100 cm depth. A Vaisala CO₂ probe (GMM220 with CARBOCAP adaptor) was installed at 50 cm, powered by an independent 30 W solar panel and 44 A-h battery. A tipping bucket rain gauge (S-RGB-M002), air temperature/relative humidity (S-THB-M002, installed within radiation shield), and insolation sensors (S-LIB-M003) were mounted 2 m above the ground. Data were recorded at 15 min intervals by the U30/NRC units. One Onset microstation data logger (model H21-002) was installed at 4700 m with soil temperature sensors (S-TMB-M006) and soil moisture sensors (S-SMD-M005) at depths of 10 and 50 cm.

3.2. Laboratory methods

In preparation for radiocarbon dating and stable isotope analysis, pedogenic carbonate samples were cleaned with a fine brush and DI water to remove soil/organic matter. The carbonate pendants were sampled using a rotary drill with a diamond-tipped bit. The powder from multiple clasts collected from the same depth was homogenized using a mortar and pestle.

Radiocarbon dating of soil carbonate samples was performed by Direct AMS (www.directams.com). Samples were digested in 85% phosphoric acid under vacuum, and the evolved CO₂ was transferred to a reaction vessel containing zinc and an inner vial of iron dust using a disposable manifold. Graphite formed after heating to 550 °C and baking for ∼5 h. The accelerator mass spectrometer analyses were performed on a National Electrostatics Corporation 1.55DH-1 Pelletron Accelerator, which produces measurements at 0.3% precision and accuracy.

Clumped isotope analyses ($\delta^{18}\text{O}$, $\delta^{13}\text{C}$ and Δ_{47}) were done at the University of Washington's IsoLab. Carbonate samples (6–8 mg) were digested in a common bath of phosphoric acid (specific gravity 1.9–1.95) held at 90 °C. The evolved CO₂ was cryogenically separated from water on an automated stainless steel vacuum line using an ethanol-dry ice slush trap, isolated in a liquid N₂ trap, and passed through a Porapak Q trap (50/80 mesh, 15 cm long, 4.5 mm ID, 0.635 mm OD) held between −10 °C and −20 °C. The CO₂ was

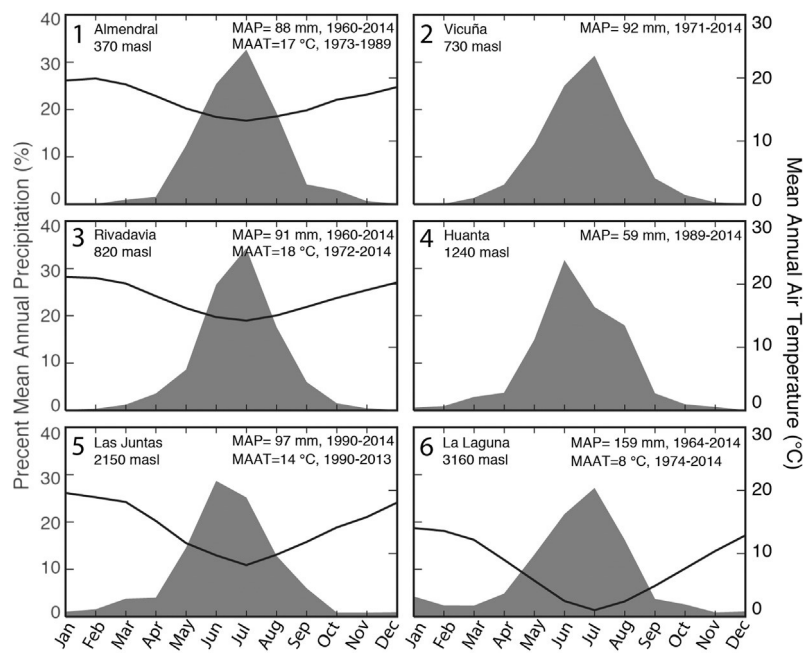


Fig. 2. Monthly percent mean annual precipitation (MAP, shaded area), and mean annual air temperature (MAAT, black line) for the weather stations maintained by the Chilean government in the Elqui valley. Years of record from DGA are labeled on the figures. At all stations, more than 60% of the total annual precipitation falls during the austral winter (JJAS).

transferred through the Porapak Q trap using He carrier gas, isolated cryogenically and transferred into a Pyrex break seal. Every 4–5 carbonate sample unknowns, a carbonate standard (NBS-19, or C64 reagent-grade calcite intralaboratory standard) or CO₂ reference frame gas was purified on the vacuum line and transferred into a Pyrex break seal. The reference frame gases were created by equilibrating CO₂ in Pyrex break seals with water of different isotopic composition held at 4 °C or 60 °C, or by heating CO₂ in quartz break seals in a muffle furnace at 1000 °C. Break seals containing purified CO₂ were loaded into an automated 10-port tube cracker inlet system on a Thermo MAT 253 configured to measure m/z 44–49 inclusive.

Δ_{47} , $\delta^{13}\text{C}$, and $\delta^{18}\text{O}$ values were calculated from the mass spectrometer data using established methods (Huntington et al., 2009 and reference therein). Δ_{47} values were corrected to the Absolute Reference Frame (ARF) of Dennis et al. (2011) using heated gas and CO₂-water equilibration lines constructed during the corresponding analysis period. $\delta^{13}\text{C}$ was referenced to the international standards NBS-19 and LSVEC, and $\delta^{18}\text{O}$ was referenced to NBS-18 and NBS-19. Samples with Δ_{48} values higher than 2‰, indicating contamination, were rejected. Following Zaarur et al. (2013), the Pierce outlier test was used to identify and remove statistical outliers in the Δ_{47} , $\delta^{13}\text{C}$, and $\delta^{18}\text{O}$ datasets.

Currently, multiple $\Delta_{47} - T$ calibrations exist and the choice of which calibration to employ can have a significant impact on the resulting carbonate $T(\Delta_{47})$ values (Defliese et al., 2015). Because our clumped-isotope analyses are most similar to the methods used by Kluge et al. (2015) and references therein, we applied the 90 °C Kluge et al. (2015) calibration (Equation (5)) to calculate $T(\Delta_{47})$; for reference, $T(\Delta_{47})$ results calculated using the Zaarur et al. (2013) calibration are given in Table 2.

To confirm the measurements of $\delta^{18}\text{O}$ and $\delta^{13}\text{C}$ made during clumped isotope analysis, repeat analyses of some samples were conducted at IsoLab using an automated Kiel III carbonate device connected to a Thermo-Finnigan Delta Plus isotope ratio mass spectrometer, following the methods detailed in Tobin et al. (2011).

Surface water and precipitation samples were analyzed on a Picarro L2130-i at Syracuse University. The isotopic values of unknown samples are reported relative to in-house standards ("Syracuse Snow" and "boiled water") calibrated against SLAP and VS-MOW international standard material. Analytical uncertainty is $\pm 2\text{\textperthousand}$ for δD and $\pm 0.2\text{\textperthousand}$ for $\delta^{18}\text{O}$ based on long-term, repeat measurement of in-house standards.

Carbonate radiocarbon ages ($n = 7$) for the soil carbonate samples range between 350 ± 30 and 9660 ± 40 yr BP (Table 2). We note that the mean radiocarbon age of soil carbonates typically underestimates the true age (Amundson et al., 1994; Wang et al., 1994), but errors in ^{14}C age estimates for soil carbonates from arid soils, such as those found in our study area, are generally smaller than the errors associated with soil carbonate from semi-humid areas (Wang et al., 1994). Our soil carbonate radiocarbon ages are younger than or coeval with the radiocarbon ages reported by Riquelme et al. (2011) for debris cones/fluvial terraces along the Elqui and Turbio rivers, and are consistent with the other geochronologic data that are available for the study area.

4. Results

4.1. Radiocarbon ages

Carbonate radiocarbon ages ($n = 7$) for the soil carbonate samples range between 350 ± 30 and 9660 ± 40 yr BP (Table 2). We note that the mean radiocarbon age of soil carbonates typically underestimates the true age (Amundson et al., 1994; Wang et al., 1994), but errors in ^{14}C age estimates for soil carbonates from arid soils, such as those found in our study area, are generally smaller than the errors associated with soil carbonate from semi-humid areas (Wang et al., 1994). Our soil carbonate radiocarbon ages are younger than or coeval with the radiocarbon ages reported by Riquelme et al. (2011) for debris cones/fluvial terraces along the Elqui and Turbio rivers, and are consistent with the other geochronologic data that are available for the study area.

4.2. Meteorological station temperature, precipitation, and CO₂ data, and vegetation survey

Mean temperatures from the weather stations installed in 2014 are within 2σ of the long-term averages measured by the DGA stations. We do not report results from the 1300 m station due to sensor malfunctions caused by vandalism. At all stations mean summer soil temperatures are elevated above MAAT (Table 3). Between the 400 and 3550 m stations mean summer soil temperature at 50 cm falls from 21 to 7 °C. The range in 2014 monthly average air temperatures ranges from ~6 °C at the 400 m station to ~10 °C at the 1900, 2700, and 3550 m stations. The range in monthly average soil temperatures is greatest at 10 cm (15–19 °C). At 100 cm, the range in monthly average soil temperatures is <14 °C. Diurnal variations in soil temperatures are greatest during the summer at shallow soil depths.

Total precipitation recorded by our stations in 2014 was extremely low compared to the long-term averages and 2014 values

Table 2
Location, stable isotope, and clumped isotope data for samples collected between 50 and 100 cm depth.

Sample ID	Latitude (°N)	Longitude (°E)	Elevation (m)	Depth (cm)	n	$\delta^{13}\text{C}$ (‰) ^a	$\pm 1\text{ SE}$ (‰) ^c	$\delta^{18}\text{O}_{\text{carb}}$ (‰) ^a	$\pm 1\text{ SE}$ (‰) ^c	$\delta^{18}\text{O}_{\text{fw}}$ (‰) ^b	$\pm 1\text{ SE}$ (‰) ^c	$T(\Delta_{47})$ (°C) ^c	$\pm 1\text{ SE}$ (°C) ^c	$T(\Delta_{47})$ Zaatur	Radiocarbon age (BP)	
Elq13-400-70	-29.9732	-70.9536	400	70	2	-7.50	0.09	-3.21	0.10	-0.55	0.619	0.030	26	11	25	7324±40
Elq13-400-95	-29.9732	-70.9536	400	95	4	-8.57	0.03	-3.39	0.07	-1.44	0.629	0.014	23	5	23	
Elq13-600-50	-30.0451	-70.8191	600	50	5	-5.91	0.03	-7.56	0.07	-3.82	0.602	0.012	32	5	29	
Elq13-650-50	-29.9876	-70.5694	850	50	7	-3.04	0.02	-6.37	0.06	-3.78	0.620	0.011	26	4	25	2873±30
Elq13-1300-60	-29.8576	-70.3649	1300	60	6	-3.57	0.03	-9.77	0.06	-7.26	0.621	0.011	26	4	25	1143±30
Elq13-1300-80	-29.8576	-70.3649	1300	80	4	-2.78	0.03	-10.46	0.07	-7.21	0.609	0.014	29	5	28	
Elq13-1300-100	-29.8576	-70.3649	1300	100	4	-3.26	0.07	-10.63	0.07	-6.68	0.599	0.014	33	5	30	
Elq13-1500-50	-29.9323	-70.2940	1500	50	6	-0.27	0.03	-9.68	0.06	-6.16	0.606	0.011	31	4	29	
Elq13-1700-50	-29.9828	-70.2333	1700	50	4	-3.31	0.04	-11.72	0.07	-8.83	0.615	0.014	28	5	26	
Elq13-1924-60	-29.9543	-70.1754	1924	60	5	-0.57	0.03	-10.24	0.07	-6.96	0.609	0.012	30	5	28	1452±30
Elq13-1924-80	-29.9543	-70.1754	1924	80	5	-1.57	0.03	-10.63	0.07	-6.38	0.595	0.012	35	5	31	
Elq13-1924-100	-29.9543	-70.1754	1924	100	4	-2.25	0.03	-11.07	0.07	-6.74	0.593	0.014	35	5	32	
Elq13-2100-50	-29.9747	-70.0984	2100	50	3	0.24	0.04	-11.49	0.09	-7.88	0.604	0.016	31	6	29	
Elq13-2300-50	-30.0532	-70.0954	2300	50	3	0.24	0.04	-13.42	0.09	-10.83	0.619	0.016	26	6	25	
Elq13-2700-60	-30.1372	-70.0624	2700	60	4	2.88	0.03	-12.65	0.07	-9.46	0.610	0.014	29	5	27	
Elq13-2700-80	-30.1372	-70.0624	2700	80	5	2.45	0.03	-13.47	0.07	-11.53	0.629	0.012	23	4	23	
Elq13-2700-100	-30.1372	-70.0624	2700	100	3	2.46	0.04	-13.47	0.09	-9.98	0.606	0.016	31	6	29	
Elq13-3100-50	-30.1939	-70.0459	3100	50	5	-4.29	0.04	-15.22	0.07	-9.31	0.570	0.012	44	5	38	
Elq13-3300-50	-30.2715	-69.9734	3300	50	4	5.81	0.03	-10.16	0.07	-11.91	0.688	0.014	6	4	10	
Elq13-3550-60	-30.2624	-69.9415	3550	60	6	1.19	0.13	-9.81	0.06	-10.78	0.675	0.012	9	4	13	5780±30
Elq13-3550-80	-30.2624	-69.9415	3550	80	4	3.93	0.09	-8.90	0.11	-9.43	0.668	0.014	11	4	14	
Elq13-3550-100	-30.2624	-69.9415	3550	100	4	0.61	0.06	-11.30	0.09	-10.25	0.643	0.014	19	5	20	
Elq13-3750-50	-30.2064	-69.9161	3750	50	5	0.87	0.03	-11.59	0.11	-13.24	0.686	0.012	6	4	10	2336±30
Elq13-4200-50	-30.1637	-69.8620	4200	50	4	6.87	0.04	-4.60	0.07	-6.47	0.689	0.014	5	4	10	9663±40
Elq13-4500-50	-30.1382	-69.8298	4500	60	6	9.12	0.05	-9.17	0.06	-12.67	0.717	0.012	-2	3	4	
Elq13-4700-60	-30.1766	-69.8295	4700	60	4	10.03	0.03	-4.20	0.07	-4.59	0.666	0.014	12	4	15	345±30
Elq13-4700-80	-30.1766	-69.8295	4700	80	4	10.46	0.03	-5.23	0.07	-6.15	0.674	0.014	10	4	13	
Elq13-4700-100	-30.1766	-69.8295	4700	100	5	9.31	0.05	-6.38	0.07	-6.66	0.664	0.012	12	4	15	

^a Carbonate $\delta^{13}\text{C}$, $\delta^{18}\text{O}$, and Δ_{47} reported as mean of n replicates.

^b Soil water $\delta^{18}\text{O}$ was calculated following the method outlined in Kim and O'Neil (1997).

^c SE was calculated by choosing whichever was larger: σ of the sample replicate measurements, or σ of the long-term CG4 in-house standard; the resulting σ was then divided by the square root of n; the $T(\Delta_{47})$ SE estimate also includes a propagation of the uncertainties associated with the $T - \Delta_{47}$ calibration of Kluge et al. (2015) (Eq. (5)).

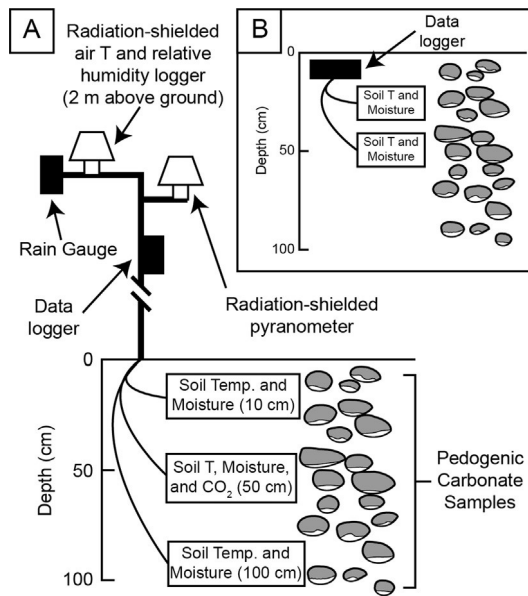


Fig. 3. Diagram of (A) the air and soil weather stations installed at 400, 1300, 1900, 2700, and 3550 masl (modified from Peters et al., 2013), and (B) soil temperature and moisture monitoring station installed at 4700 masl (modified from Ringham et al., 2016).

recorded by the DGA stations (Table 3). For sites >2700 m this discrepancy may be due in part to the type of rain gauge we used, which does not accurately measure snowfall. As shown in Fig. 4, the 400 m station received the most rain (0.5 mm; 3 events), while 0.3 mm (3 events) fell at 1900 m, 0.2 mm (2 events) fell at 2700 m, and no rain fell at the 3550 m station. The DGA rain gauges show rainfall events in the same months; however, the DGA stations recorded one to two orders of magnitude more precipitation (1–10 s of mm) than our rain gauges.

Soil $p\text{CO}_2$ was low at all stations, ranging from 22 to 451 ppm at the 2700 m station. The CO_2 sensors installed at the 3500 m site did not function properly and failed to log any measurements.

Our study area is dominated by C_3 vegetation, with no significant C_4 or CAM biomass (this study and Marticorena et al., 2001). The few CAM plants (e.g., *Echinopsis* cacti) found in the area are restricted to lower elevation sites (<2000 m). In general, vegetation richness decreases with elevation. Around 400 m *Eulychnia* and *Echinopsis* cacti dominate the xerophytic scrub. From 1000 to 2000 m the vegetation has low cover and is dominated by sub-shrubs such as *Encelia*, *Adesmia* and a few *Stipa* grasses. At 2700 m, desert shrubs (*Ephedra*, *Fabiana*, *Atriplex* and *Adesmia*) dominate the landscape. Above 3500 m, the Andean steppe is characterized by grasses including *Stipa*, some sub-shrubs such as *Phacelia* and some cushion *Adesmia* and a 50% plant cover, until the vegetation limit at ~4300 m (0% cover).

4.3. $\delta^{18}\text{O}$, $\delta^{13}\text{C}$, and $T(\Delta_{47})$ results

Water isotope values from collectors mounted at DGA precipitation gauges, streams and snowpack (Fig. 6A; Table SI1 in the Supplementary Information) range from -18.1 to $-1.9\text{\textperthousand}$ and decrease by $\sim 1.9\text{\textperthousand km}^{-1}$ with elevation. Amount-weighted means are calculated for rainfall isotope data; however, we note that the precipitation measurements represent just 2 years of data collection during a prolonged drought and are limited to a small number of samples below 3100 m and thus may not be representative of the long-term precipitation $\delta^{18}\text{O}$ values.

Soil carbonate $\delta^{18}\text{O}$, $\delta^{13}\text{C}$, and $T(\Delta_{47})$ results are reported in Table 2 and Table SI2 in the Supplementary Information. The $\delta^{18}\text{O}$ values (VPDB) of all samples range from -3.2 to $-15.2\text{\textperthousand}$, and

Table 3
Weather stations installed for this study. Data collected from Jan. 2014 to Jan. 2015.

Stations ^{a,b}	Latitude (°N)	Longitude (°E)	Elevation (m)	Total precip. (mm)	Air temp. (°C)	10 cm soil temp. (°C)		50 cm soil temp. (°C)		100 cm soil temp. (°C)	
						Mean annual	Mean summer	Mean winter	Mean annual	Mean summer	Mean winter
1	-29.9732	-70.9536	400	0.5	14.4	11.8	21.0	28.8	14.2	21.2	15.7
3	-29.9543	-70.1754	1924	0.3	16.1	11.6	20.8	29.1	13.2	20.9	14.6
4	-29.848	-70.385	2700	0.2	10.7	16.4	6.1	13.9	5.0	14.3	22.8
5	-30.2624	-69.9415	3550	0	3.7	9.7	0.1	6.7	0.8	7.4	14.8
6	-30.1766	-69.8295	4700	NA	NA	NA	NA	-0.7	9.1	-8.2	-0.3
									7.8	7.8	-6.2

^a Station 2 (at 1300 masl) was vandalized; the results from that station are not included in this table.

^b Station number corresponds to the black numbered circles in Fig. 1.

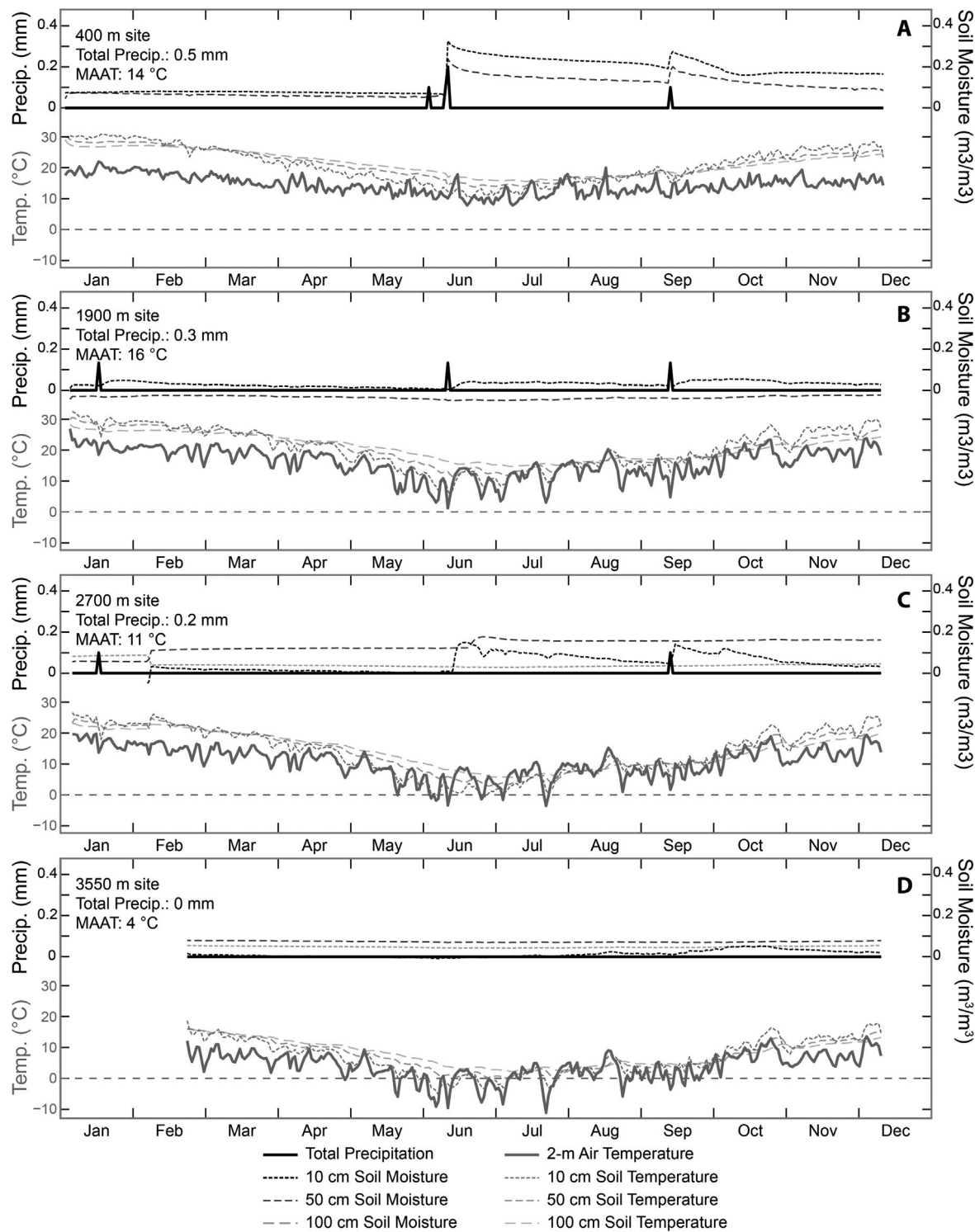


Fig. 4. Weather station data for the six stations installed as part of this study at the 400, 1900, 2700 and 3550 masl sites. Data covers the period January 3 to December 11, 2014.

$\delta^{13}\text{C}$ values (VPDB) range from -8.6 to $10.5\text{\textperthousand}$, with a mean standard error (SE) of $\pm 0.01\text{\textperthousand}$. For the 1-m soil pits, $\delta^{18}\text{O}$ and $\delta^{13}\text{C}$ values increase towards the surface and are generally invariant below 40 cm depth (Fig. 5). The mean $\delta^{18}\text{O}$ values of samples collected at depths >40 cm range from $-13.2\text{\textperthousand}$ at the 2700 m soil profile, to $-5.3\text{\textperthousand}$ at the 4700 m profile. The mean $\delta^{13}\text{C}$ values of samples collected at >40 cm depth range from $-8.0\text{\textperthousand}$ at the 400 m soil profile, to $9.9\text{\textperthousand}$ at 4700 m. We used the carbonate $T(\Delta_{47})$ and $\delta^{18}\text{O}$ values to reconstruct soil water $\delta^{18}\text{O}$ values (Kim and

O'Neil, 1997). The calculated soil water $\delta^{18}\text{O}$ values are 0 to 5\textperthousand higher than the $\delta^{18}\text{O}$ values of local surface water as measured in this study and in Strauch et al. (2006); as an exception, the 4700 m sample values are $\sim 14\text{\textperthousand}$ higher than local surface water $\delta^{18}\text{O}$ values (Fig. 6A).

Carbonate $\delta^{13}\text{C}$ values increase with elevation, from $-8.6\text{\textperthousand}$ at 400 m to $10.5\text{\textperthousand}$ at 4700 m. Below 2500, most of the samples fall between the expected values of carbonates formed in isotopic equilibrium with atmospheric CO₂ (-6.5 to $-8.5\text{\textperthousand}$, pre-industrial

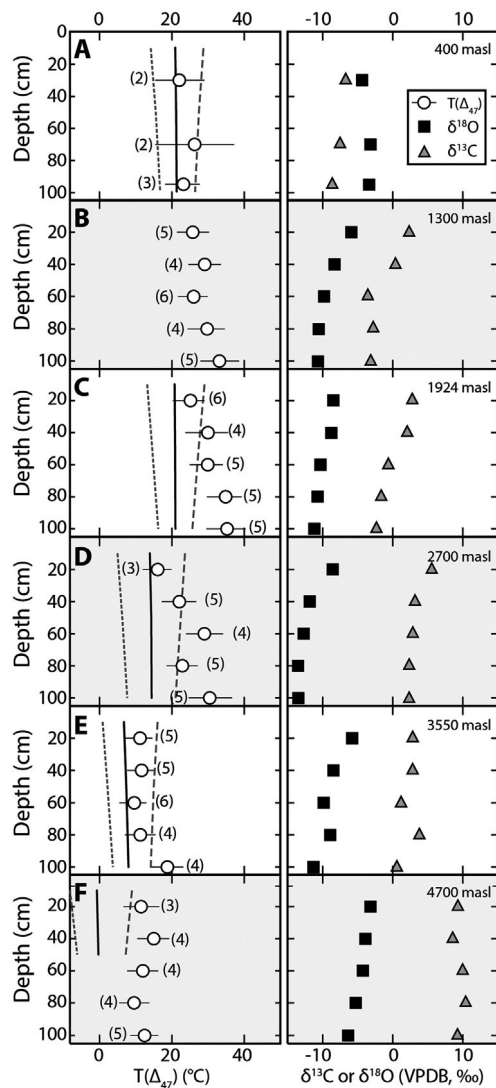


Fig. 5. Depth profiles showing soil carbonate $T(\Delta_{47})$ (left column) and $\delta^{18}\text{O}$ and $\delta^{13}\text{C}$ (right column, VPDB) results for the five 1-m depth soil pits. The number of replicate analyses for each sample is indicated in parentheses. Lines show the mean annual (black), summer (dashed), and winter (dotted) soil temperatures from Jan. 2014 to Jan. 2015. Due to equipment failure, soil temperatures are not available for the 1300 masl site.

and modern, respectively) and with CO_2 gas respired from C_3/CAM plants (minimum $\delta^{13}\text{C} = \text{approximately } -25\text{\textperthousand}$) (Breecker et al., 2009; Cerling and Quade, 1993; Diefendorff et al., 2010; Kohn, 2010; Quade et al., 2007a, 2007b). Above 2500 m, the $\delta^{13}\text{C}$ values of several samples exceed the expected values of carbonates that formed in isotopic equilibrium with the pure atmosphere (Fig. 6B). The 50 cm sample collected at 3100 m has an anomalously low value ($-4.3\text{\textperthousand}$) compared to neighboring samples.

$T(\Delta_{47})$ values range from -2°C to 35°C , with one outlier at 44°C from the sample collected at 3100 m, which will be treated as an outlier for purposes of interpretation. After accounting for uncertainties in external replicate measurements and the Kluge et al. (2015) $T - \Delta_{47}$ calibration, the mean external error in temperature is $\pm 5^\circ\text{C}$ (1 standard error). Samples collected from below 3200 m elevation yield $T(\Delta_{47})$ values greater than mean summer soil temperatures at all depths, although shallow samples (20 and 40 cm) are consistently colder than deeper samples. At elevations >3200 m, sample $T(\Delta_{47})$ values fall within the expected range of Holocene MAST (Fig. 7). In contrast to the other high elevation samples, the samples collected at the highest site (4700 m) yielded

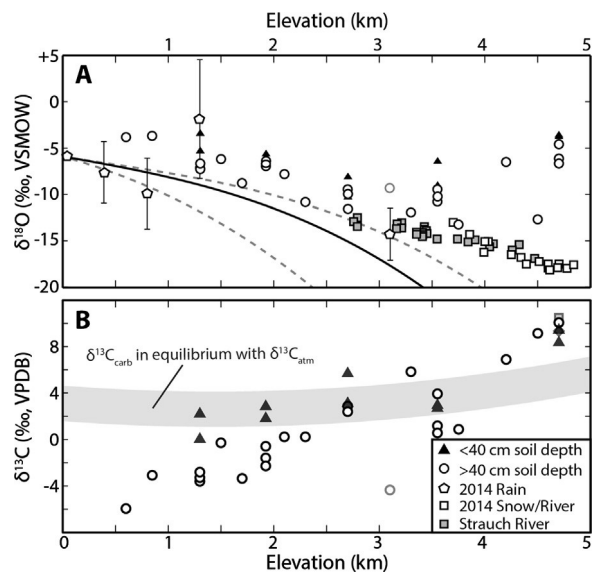


Fig. 6. Calculated soil water $\delta^{18}\text{O}$ and soil carbonate $\delta^{13}\text{C}$ results versus elevation. A) Calculated soil water $\delta^{18}\text{O}$ values are shown for samples collected at depths <40 (black triangles) and >40 cm (white circles). Measured $\delta^{18}\text{O}$ values of 2014 precipitation (white pentagons) are shown with 1 SE error bars. Note that MAP in 2014 was extremely low, and these measurements represent a relatively small sample size. 2014 river, stream and snowpack samples are denoted by the white squares. Water samples were collected during the 2013 field season. River water samples collected by Strauch et al. (2006) are shown for comparison (gray squares). The black line represents a calculated precipitation fractionation pathway calculated using the model described in Rowley et al. (2001). Dashed gray lines mark the 1 SE uncertainty in modeling results. B) Soil carbonate sample $\delta^{13}\text{C}$ values at <40 cm depth (black triangles) and >40 cm depth (white circles) are plotted vs. elevation; the shaded region marks the expected composition of carbonate that has formed in equilibrium with pure atmospheric CO_2 (based on Holocene atmospheric CO_2 values of -8.5 to $-6.5\text{\textperthousand}$), based on estimated mean annual air temperature variations over the past 20 kyr (Kaiser et al., 2008) and on the temperature-dependent fractionation between $\text{CO}_2(\text{g})$ and CaCO_3 at 25 and 0°C (Romanek et al., 1992).

an apparent $T(\Delta_{47})$ value of 9°C , which is within error of mean summer soil temperatures observed at that location.

5. Discussion

5.1. Comparing soil carbonate $T(\Delta_{47})$, $\delta^{18}\text{O}$ and $\delta^{13}\text{C}$ to modern environmental parameters

To determine if changes to soil moisture conditions affect the seasonal biases of soil carbonate formation and the resulting $T(\Delta_{47})$ values, we compare our sample $T(\Delta_{47})$ values to modern temperature and precipitation records. Due to the limited temporal coverage of meteorological datasets compared to the long timescale of soil carbonate formation we discuss how soil temperatures varied over the past ~ 20 kyr. Since the Late Pleistocene, regional MAAT was no more than 4°C cooler and 2°C warmer than the present (Kaiser et al., 2008), and we account for this expected range of Holocene soil temperatures in our figures by displaying uncertainties of -4 and $+2^\circ\text{C}$ around the measured 2014 soil temperatures. Despite long-term increases and decreases in precipitation over the past 20 kyr, the region was consistently arid (Lamy et al., 1999). Dating on moraines north of the study area (29°S), suggests that the equilibrium line altitudes of nearby glaciers have experienced a net change of <500 m since the Late Pleistocene (Grosjean et al., 1998). LANDSAT imagery since 1975 shows that above 3200 m winter precipitation falls predominantly as snow, while lower elevations receive mainly rain (LANDSAT 1–5 MSS, 4–5 TM, and 7 ETM images courtesy of the USGS, www.earthexplorer.usgs.gov). Together, these observations imply

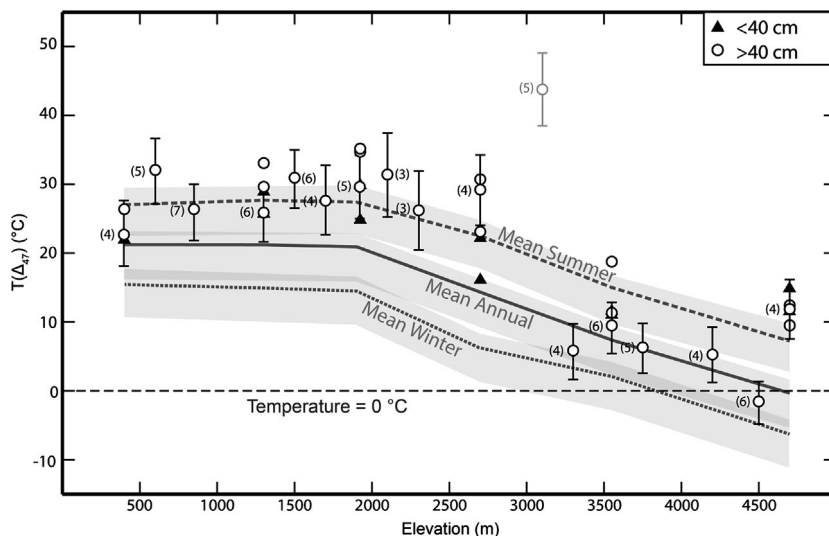


Fig. 7. Mean $T(\Delta_{47})$ results versus elevation for samples collected at depths <40 cm (gray triangles) and at depths >40 cm (black circles). The numbers in parentheses indicate the number of replicates per sample for the 50 and 60 cm samples. The error bars show the ± 1 SE about the mean for the 50/60 cm samples (95 cm sample at the 400 m site). Grey lines show the mean annual (solid), mean summer (dashed), and mean winter (dotted) soil temperatures at 50 cm depth measured from Jan. to Dec. 2014; horizontal dashed black line marks 0°C . The shaded regions around the mean summer, annual and winter lines show the expected range of Holocene mean, summer and winter soil temperatures (see text for explanation).

that the winter snow line elevation has probably varied <500 m during the Holocene.

The limited amount of precipitated water collected from the DGA weather stations during 2013 makes it difficult to determine if the low-elevation precipitation $\delta^{18}\text{O}$ values are representative of mean meteoric water $\delta^{18}\text{O}$; however the $\delta^{18}\text{O}$ values of river and stream samples at higher elevations are in line with isotopic measurements conducted by previous studies (Fig. 6A). Long-term measurements of precipitation measured at the La Serena Global Network of Isotopes in Precipitation (GNIP) station yield a mean $\delta^{18}\text{O}$ of $-5.9\text{\textperthousand}$ (Table S1; IAEA/WMO, 2016) and provide a starting point for modeling a hypothetical fractionation pathway of precipitation using the model developed by Rowley et al. (2001), with an assumed starting temperature of 14°C (mean temperature from May to August) and relative humidity = 81%. At elevations below ~ 3200 m the $\delta^{18}\text{O}$ values of reconstructed soil water are slightly enriched in ^{18}O above both meteoric water samples and the modeled precipitation $\delta^{18}\text{O}$ values, suggesting the soil waters experience at least some evaporative enrichment (Liu et al., 1996). Above 3200 m, the $\delta^{18}\text{O}$ value of river and stream samples continues to decrease, while the reconstructed soil waters display a high degree of variability.

Carbonate $\delta^{13}\text{C}$ values increase with elevation, and above 4000 m plot above the expected range of $\delta^{13}\text{C}$ values for hypothetical Holocene carbonates that formed in equilibrium with pure atmospheric CO_2 (Fig. 6B, dark gray band), taking into account the temperature-dependent fractionation between CO_2 and calcite (Romanek et al., 1992; Cerling and Quade, 1993). Even at the lowest elevation study sites, carbonate $\delta^{13}\text{C}$ values are higher than would be expected for pure C_3 vegetation, suggesting that local aridity and the presence of some CAM plants (e.g., *Echinopsis* cacti) leads to a more ^{13}C -enriched soil CO_2 . At higher elevations the total vegetation cover decreases, causing atmospheric CO_2 to dominate the soil CO_2 composition and an increase in carbonate $\delta^{13}\text{C}$ values.

After accounting for the evaporative effect in this arid region (higher $\delta^{18}\text{O}$) and soil productivity that is low and decreases with increasing elevation (higher $\delta^{13}\text{C}$; Cerling and Quade, 1993; Kohn, 2010), most sample data are consistent with the soil carbonates having formed under apparent isotopic equilibrium with local soil water and soil CO_2 (Fig. 6). In contrast, samples from the highest site (4700 m) yield apparent $T(\Delta_{47})$ values much higher than other nearby samples, calculated soil water $\delta^{18}\text{O}$ values up to

14‰ higher than local waters, and $\delta^{13}\text{C}$ values enriched by up to 4‰ above the estimated isotopic composition of Holocene atmospheric CO_2 .

5.2. Systematic changes in soil carbonate $T(\Delta_{47})$ due to changes in soil moisture

Soil carbonate $T(\Delta_{47})$ values show a clear change in seasonal bias at ~ 3200 m (Fig. 7), coinciding with the mean position of the winter snow line. $T(\Delta_{47})$ values below 2700–3200 m generally match or exceed the expected range of Holocene mean summer soil temperatures. $T(\Delta_{47})$ values from elevations of 3200 to 4500 m are within error of Holocene MAST. The high $T(\Delta_{47})$ values for samples collected below 3200 m at depths >40 cm agree with other studies that observed summer formation biases in soil carbonates collected from arid climates (Hough et al., 2014; Passey et al., 2010; Peters et al., 2013; Quade et al., 2013; Ringham et al., 2016). However, the $T(\Delta_{47})$ values of soil carbonates collected at depths <40 cm are more variable (Figs. 5 and 7), with samples generally yielding $T(\Delta_{47})$ values cooler than mean summer soil temperature. We propose that this discrepancy between shallow and deep soil carbonate $T(\Delta_{47})$ values is due to two mechanisms: 1) only the largest precipitation events lead to infiltration of meteoric water to depths >40 cm; once wet, these deeper soils only dry out during the hottest summer months; and 2) rapid growth of soil carbonates occurs at shallow depths during short-term periods of soil temperature depression following small precipitation events.

Recent work in Argentina has shown that small rain events are unlikely to penetrate deeply into arid soils (Ringham et al., 2016). Thus, deep horizons (>40 cm) in the soil profile may only be wetted infrequently, and once wet, these horizons may remain too moist for carbonate precipitation until drying occurs in the warm late spring and summer. This is consistent with soil moisture data from our 400 m and 1900 m sites, which both recorded a wetting event in early June 2014 (austral winter). At the 400 m site, the rainfall event was large enough to show increases in soil moisture at 10 and 50 cm depths, which remained elevated well into the summer months (Fig. 4); however, at the 1900 m site, the recorded rain event was smaller, and an increase in soil moisture was only recorded at 10 cm.

In light of these observations, we propose the following process for carbonate precipitation at elevations <3200 m: 1) winter rainfall causes increases in soil moisture, with the soil moisture of deeper soil horizons only increasing during the largest rain events; 2) relatively fast drying of shallow (<40 cm depth) soil horizons due to evaporation following smaller rain events leads to soil carbonate precipitation during the period of cooler shallow soil temperatures that are observed immediately after most precipitation events (Ringham et al., 2016), resulting in variable, cooler, soil carbonate $T(\Delta_{47})$ values; 3) relatively slow drying of deeper soil horizons following larger rain events causes calcite supersaturation of deeper soil waters only after prolonged periods of high temperature, resulting in soil carbonate $T(\Delta_{47})$ values that are biased towards mean summer soil temperature.

The transition from warm-biased $T(\Delta_{47})$ values below 2700–3200 m to $T(\Delta_{47})$ values that resemble MAST at higher elevations (Fig. 7) coincides with the average position of the winter snowline. The presence of winter snow could cause colder $T(\Delta_{47})$ values via one of two mechanisms: 1) soil carbonate formation may be restricted to the brief period of time between soil wetting and drying. If this is the case, then soil carbonate formation at depths <40 cm in the soil profile may occur rapidly following the onset of melting, leading to $T(\Delta_{47})$ values that are biased towards cold (near 0 °C) temperatures due to heat advection by melt water. 2) The presence of a snow layer and the initiation of snowmelt in the spring could affect the timing and rate of soil drying (Rodhe, 1998), causing a change in the seasonality of carbonate formation. We favor the second explanation for two reasons. First, the $T(\Delta_{47})$ values of the >3200 m samples are generally warmer than 0 °C. Second, soil moisture data from the 3550 m site shows maximum drying during the austral autumn (Fig. 4D), and the expected range of Holocene autumn soil temperatures agrees well with MAST and the measured $T(\Delta_{47})$ values.

We interpret our data to suggest that the timing of soil moisture wetting and drying events have a large impact on seasonal biases in soil carbonate formation and $T(\Delta_{47})$ values. This is consistent with Peters et al. (2013), who suggested that changes to the seasonality of precipitation can lead to changes in the seasonal biases of soil carbonate $T(\Delta_{47})$ values.

5.3. High-elevation cryogenic carbonate formation

There are several possible explanations for the anomalously high $T(\Delta_{47})$, $\delta^{18}\text{O}$ and $\delta^{13}\text{C}$ values observed at the 4700 m sample site. Repeated cycles of carbonate dissolution and precipitation can lead to enrichment of carbonate $\delta^{13}\text{C}$ (Clark and Lauriol, 1992); however, low soil moisture values (<0.12 m³ m⁻³), and reports of persistent, high calcite activity values ($\alpha_{\text{calcite}} < 1$) from similar environments in Argentina (Ringham et al., 2016) suggest that dissolution of soil carbonates is rare. Aridity effects on soil respiration and evaporation can lead to significant increases in both $\delta^{18}\text{O}$ and $\delta^{13}\text{C}$ values of soil carbonate. Quade et al. (2007b) report estimated soil water $\delta^{18}\text{O}$ enrichments of up to 10‰ compared to local rainwater in the Atacama Desert (+700 km north of the Elqui Valley), and soil carbonate $\delta^{13}\text{C}$ values of up to +7.3‰; however, the high-elevation regions of our study area are less arid than the Atacama Desert but the calculated soil water $\delta^{18}\text{O}$ enrichment and $\delta^{13}\text{C}$ values of our 4700 m carbonates are even higher than carbonates collected from the Atacama. Sublimation of snow/ice prior to meltwater infiltration may be responsible for some of the observed $\delta^{18}\text{O}$ enrichment at the 4700 m site (Lechler and Niemi, 2011), but this does not explain the elevated carbonate $\delta^{13}\text{C}$ values.

We hypothesize that both the extremely high soil carbonate $\delta^{18}\text{O}$ and $\delta^{13}\text{C}$ values and relatively low Δ_{47} values at 4700 m can be explained by kinetic isotope effects (KIE) associated with cryogenic carbonate formation. Cryogenic soil carbonates pre-

cipitate when a soil water solution reaches calcite supersaturation due to the exclusion of solute ions from the ice matrix, and can form under non-equilibrium conditions with respect to soil water and soil CO₂ (Courty et al., 1994; Kluge et al., 2014; Lacelle, 2007). Environmental conditions unique to the 4700 m site may explain why cryogenic carbonates are found at this site. The area is devoid of vegetation and the soil matrix is composed of ~3 cm unconsolidated clasts, which may affect the ability of the soil to retain moisture throughout the year. Perennial snow fields partially cover the area.

The KIE associated with cryogenic carbonate formation are the result of rapid CO₂ degassing via bicarbonate dehydration and dehydroxylation, induced by fast solution freezing (Clark and Lauriol, 1992; Guo, 2009). Due to the differences in zero-point energy levels, dehydration of bicarbonate isotopologues containing ¹²C and ¹⁶O proceeds faster than the dehydration of isotopologues containing ¹³C and ¹⁸O, resulting in a dissolved inorganic carbon (DIC) pool with higher $\delta^{13}\text{C}$ and $\delta^{18}\text{O}$ values (degassed CO₂ with lower $\delta^{13}\text{C}$ and $\delta^{18}\text{O}$ values; Clark and Lauriol, 1992). This process causes lower carbonate Δ_{47} values (higher $T(\Delta_{47})$ values) because degassing CO₂ from a bicarbonate solution acts as a “reverse” mixing problem (Guo, 2009). Previous studies have shown that mixing two end member CO₂ pools with distinct bulk isotope compositions but identical Δ_{47} compositions produces a combined CO₂ pool with a Δ_{47} composition that is not a simple linear mixture of the two original pools (Eiler and Schäuble, 2004; Defliese and Lohmann, 2015). In a similar way, degassing isotopically light CO₂ results in a new, lower Δ_{47} value for the remnant DIC pool (Guo, 2009).

Our findings are consistent with experiments conducted by Tripathi et al. (2015), which suggest that CO₂ dehydration and dehydroxylation lead to $\delta^{18}\text{O}$ enrichment and Δ_{47} depletion in the resulting carbonate. The data from the 4700 m site show that for every 1‰ increase in $\delta^{18}\text{O}$ with respect to local surface waters, Δ_{47} decreases by ~0.001‰ with respect to the expected Δ_{47} of carbonates formed under equilibrium conditions in the same water. This Δ_{47} – $\delta^{18}\text{O}$ relationship is less than that reported by Guo (2009) (0.02 to 0.026‰ decrease in Δ_{47} for every 1‰ increase in $\delta^{18}\text{O}$), and nearer that reported by Kluge et al. (2014) for cryogenic cave carbonates (0.005‰). Our findings add to the body of evidence suggesting that the $\delta^{18}\text{O}$ – Δ_{47} offset correlation in carbonates formed under non-equilibrium conditions can vary significantly (Kluge et al., 2014 and references therein).

The magnitude of kinetic fractionation observed in cryogenic carbonates depends on the rate at which the solution freezes. Clark and Lauriol (1992) suggest that freezing must occur nearly instantaneously in order for KIE to occur, but Guo (2009) observed KIE in carbonates that resulted from a bicarbonate solution that froze over the course of ~3 h. We suggest that soil water freezing at our 4700 m site proceeds unusually fast due to the open nature of the soil matrix. Using a simple heat diffusion equation (Quade et al., 2013, Eq. (1)), we estimate that bare soil at 4700 m experiences winter diurnal temperature swings of up to 12 °C at 10 cm depth, consistent with our soil temperature observations. This suggests that rapid freezing is possible near the soil surface. Our observations show smaller diurnal temperature variations at depth, but the similarity in $T(\Delta_{47})$, $\delta^{18}\text{O}$, and $\delta^{13}\text{C}$ values among soil carbonates sampled at different depths suggests that at all depths >1 m freezing still proceeds rapidly enough to produce KIE in soil carbonates.

The identification of cryogenic soil carbonates at high elevations has implications for anomalous $T(\Delta_{47})$ values from previously published datasets. Quade et al. (2011) presented $T(\Delta_{47})$ data for nine Tibetan soil carbonate samples that were collected at elevations >3800 m. Similar to our 4700 m samples, the $T(\Delta_{47})$, $\delta^{13}\text{C}$, and $\delta^{18}\text{O}$ values of these carbonates are unexpectedly high.

Based on our findings from the 4700 m site, we propose that these anomalously high $T(\Delta_{47})$ values may be due to cryogenic carbonate formation.

5.4. Biases in shallow soil carbonate $T(\Delta_{47})$ values

Our results suggest that the $T(\Delta_{47})$ values of shallow soil carbonates are poor proxies of mean annual or carbonate growth season soil temperatures. Quade et al. (2013) suggested that $T(\Delta_{47})$ values of soil carbonates formed during the warm season should systematically increase towards the surface; however, we observe the opposite: below 2700–3200 m, shallow (<40 cm) soil carbonate $T(\Delta_{47})$ values are similar to or in some cases cooler than deeper carbonates. Our findings are consistent with observations in Argentina that show soil carbonate $T(\Delta_{47})$ values on the eastern flank of the Andes are isothermal with depth (Peters et al., 2013; Ringham et al., 2016). Our soil temperature and moisture observations show that small precipitation events lead to short-term depression of soil temperatures at shallow depths in the soil profile, and taken together with the $T(\Delta_{47})$ values are consistent with the hypothesis that shallow soil carbonates tend to form soon after precipitation events when shallow (<40 cm) soil temperatures are depressed (Ringham et al., 2016). These findings suggest that shallow carbonates are not appropriate for use as paleoclimate proxies.

6. Implications and conclusions

The Elqui and Turbio valleys in north-central Chile provide an opportunity to compare the $\delta^{18}\text{O}$, $\delta^{13}\text{C}$, and $T(\Delta_{47})$ values of Holocene pedogenic carbonates collected from environments with different soil temperature and moisture conditions. At elevations <3200 m, soil carbonate $T(\Delta_{47})$ values show a warm-season bias. Above 3200 m, carbonate $T(\Delta_{47})$ values resemble MAST. We propose that the presence of snow during the winter months alters when and how rapidly soil drying occurs, resulting in cooler $T(\Delta_{47})$ values for the >3200 m samples. At our highest elevation site (4700 m) we interpret anomalously high $\delta^{18}\text{O}$ and $\delta^{13}\text{C}$ and low Δ_{47} values to reflect KIE due to cryogenic carbonate formation.

Our findings have important implications for the use of soil carbonates as paleotemperature proxies. Building previous studies (e.g., Peters et al., 2013; Hough et al., 2014), we show that seasonal biases in $T(\Delta_{47})$ are likely driven by soil moisture conditions, and that changes to seasonal soil moisture balance affect the relationship between $T(\Delta_{47})$ and MAAT. Thus, when using soil carbonate $T(\Delta_{47})$ as a paleoclimatic proxy, care should be taken to understand past soil moisture conditions.

Future work should focus on using the soil moisture indicators commonly preserved in paleosols (e.g., Mack et al., 1993; Hyland et al., 2015; Nordt and Driese, 2010; Retallack, 2005) to quantify how changes to soil moisture may have affected the $T(\Delta_{47})$ of ancient soil carbonates. To better relate our work to ancient paleosol carbonates, the methods described in this study should be applied to carbonate nodules, which are more commonly preserved in the geologic record and typically integrate a longer climate signal than pendants. Finally, we show that at high elevations, cryogenic processes can affect the bulk and clumped isotope values of soil carbonates. Identifying cryogenic soil carbonates is especially relevant for paleoelevation studies, since KIE may bias these carbonates to high $T(\Delta_{47})$ values, causing underestimates in elevation reconstructions.

Acknowledgements

We thank Carlos Galleguillos and Gustavo Freixas of the La Serena office of the Dirección General de Aguas (DGA) for permission to deploy rain collectors at DGA stations as well as providing station data. KWH and GDH were supported by NSF Grant

EAR-1252064. KWH also received support from EAR-1156134. LKB was supported by a GSA research grant from the Geological Society of America (10615-14). The authors thank Nathan Sheldon and an anonymous reviewer for their insightful and constructive comments, and Heather Stoll for editorial support.

Appendix A. Supplementary material

Supplementary material related to this article can be found online at <http://dx.doi.org/10.1016/j.epsl.2016.02.033>.

References

- Amundson, R., Wang, Y., Chadwick, O., Trumbore, S., McFadden, L., McDonald, E., Wells, S., DeNiro, M., 1994. Factors and processes governing the ^{14}C content of carbonate in desert soils. *Earth Planet. Sci. Lett.* 125 (1–4), 385–405. [http://dx.doi.org/10.1016/0012-821X\(94\)90228-3](http://dx.doi.org/10.1016/0012-821X(94)90228-3).
- Breecker, D.O., Sharp, Z.D., McFadden, L.D., 2009. Seasonal bias in the formation and stable isotopic composition of pedogenic carbonate in modern soils from central New Mexico, USA. *Geol. Soc. Am. Bull.* 121 (3–4), 630–640. <http://dx.doi.org/10.1130/B26413.1>.
- Cerling, T., Quade, J., 1993. Stable carbon and oxygen isotopes in soil carbonates. In: Swart, P.K., Lohmann, K.C., McKenzie, J., Savin, S. (Eds.), *Climate Change in Continental Isotopic Records*. American Geophysical Union, pp. 217–231.
- Clark, I.D., Lauriol, B., 1992. Kinetic enrichment of stable isotopes in cryogenic calcites. *Appl. Geochem.* 102, 217–228.
- Courty, M., Marlin, C., Dever, L., Tremblay, P., Vachier, P., 1994. The properties, genesis and environmental significance of calcitic pendants from the High Arctic (Spitsbergen). *Geoderma* 61, 71–102.
- Defliese, W., Lohmann, K., 2015. Non-linear mixing effects on mass-47 CO_2 clumped isotope thermometry: patterns and implications. *Rapid Commun. Mass Spectrom.* 29, 901–909. <http://dx.doi.org/10.1002/rcm.7175>.
- Defliese, W.F., Hren, M.T., Lohmann, K.C., 2015. Compositional and temperature effects of phosphoric acid fractionation on Δ_{47} analysis and implications for discrepant calibrations. *Chem. Geol.* 396, 51–60. <http://dx.doi.org/10.1016/j.chemgeo.2014.12.018>.
- Dennis, K.J., Affek, H.P., Passey, B.H., Schrag, D.P., Eiler, J.M., 2011. Defining an absolute reference frame for “clumped” isotope studies of CO_2 . *Geochim. Cosmochim. Acta* 75 (22), 7117–7131. <http://dx.doi.org/10.1016/j.gca.2011.09.025>.
- Diefendorf, A.F., Mueller, K.E., Wing, S.L., Koch, P.L., Freeman, K.H., 2010. Global patterns in leaf ^{13}C discrimination and implications for studies of past and future climate. *Proc. Natl. Acad. Sci.* 107 (13), 5738–5743. <http://dx.doi.org/10.1073/pnas.0910513107>.
- Drever, J.I., 1988. *The Geochemistry of Natural Waters*, 2nd ed. Prentice Hall, Englewood Cliffs, New Jersey, p. 436.
- Eagle, R.A., Risi, C., Mitchell, J.L., Eiler, J.M., Seibt, U., Neelin, J.D., Li, G., Tripati, A.K., 2013. High regional climate sensitivity over continental China constrained by glacial-recent changes in temperature and the hydrological cycle. *Proc. Natl. Acad. Sci. USA* 110 (22), 8813–8818. <http://dx.doi.org/10.1073/pnas.1213366110>.
- Eiler, J.M., 2007. “Clumped-isotope” geochemistry—the study of naturally-occurring, multiply-substituted isotopologues. *Earth Planet. Sci. Lett.* 262 (3–4), 309–327. <http://dx.doi.org/10.1016/j.epsl.2007.08.020>.
- Eiler, J.M., 2011. Paleoclimate reconstruction using carbonate clumped isotope thermometry. *Quat. Sci. Rev.* 30 (25–26), 3575–3588. <http://dx.doi.org/10.1016/j.quascirev.2011.09.001>.
- Eiler, J.M., Bergquist, B., Bourg, I., Cartigny, P., Farquhar, J., Gagnon, A., Guo, W., Halevy, I., Hofmann, A., Larson, T., Levin, N., Schable, E., Stolper, D., 2014. Frontiers of stable isotope geoscience. *Chem. Geol.* 372, 119–143. <http://dx.doi.org/10.1016/j.chemgeo.2014.02.006>.
- Eiler, J.M., Schable, E., 2004. $^{18}\text{O}^{13}\text{C}^{16}\text{O}$ in Earth's atmosphere. *Geochim. Cosmochim. Acta* 68 (23), 4767–4777. <http://dx.doi.org/10.1016/j.gca.2004.05.035>.
- Fiebig-Wittmaack, M., Astudillo, O., Wheaton, E., Wittrock, V., Perez, C., Ibacache, A., 2012. Climatic trends and impact of climate change on agriculture in an arid Andean valley. *Clim. Change* 111, 819–833. <http://dx.doi.org/10.1007/s10584-011-0200-z>.
- Garreaud, R.D., Vuille, M., Compagnucci, R., Marengo, J., 2009. Present-day South American climate. *Paleogeogr. Palaeoclimatol. Palaeoecol.* 281 (3–4), 180–195. <http://dx.doi.org/10.1016/j.palaeo.2007.10.032>.
- Garzione, C.N., Auerbach, D.J., Jin-Sook Smith, J., Rosario, J.J., Passey, B.H., Jordan, T.E., Eiler, J.M., 2014. Clumped isotope evidence for diachronous surface cooling of the Altiplano and pulsed surface uplift of the Central Andes. *Earth Planet. Sci. Lett.* 393, 173–181. <http://dx.doi.org/10.1016/j.epsl.2014.02.029>.
- Garzione, C.N., Hoke, G.D., Libarkin, J.C., Withers, S., MacFadden, B., Eiler, J., Prosenjit, G., Mulch, A., 2008. Rise of the Andes. *Science* (New York, N.Y.) 320, 1304–1307. <http://dx.doi.org/10.1126/science.1148615>.
- Ghosh, P., Adkins, J., Affek, H., Balta, B., Guo, W., Schable, E.A., Eiler, J.M., 2006a. $^{13}\text{C}-^{18}\text{O}$ bonds in carbonate minerals: a new kind of paleothermometer. *Geochim. Cosmochim. Acta* 70 (6), 1439–1456. <http://dx.doi.org/10.1016/j.gca.2005.11.014>.

- Ghosh, P., Garzione, Carmala, N., Eiler, J.M., 2006b. Rapid uplift of the Altiplano revealed through ^{13}C - ^{18}O bonds in paleosol carbonates. *Science* 311, 511–515.
- Gile, L., Peterson, F., Grossman, R., 1966. Morphological and genetic sequences of carbonate accumulation in desert soils. *Soil Sci.* 101 (5), 347–360.
- Grosjean, M., Geyh, M., Messerli, B., 1998. A late-Holocene (<2600 BP) glacial advance in the south-central Andes (29°S), northern Chile. *Holocene* 8 (4), 473–479.
- Guo, W., 2009. Carbonate clumped isotope thermometry: application to carbonaceous chondrites & effects of kinetic isotope fractionation. California Institute of Technology. Retrieved from <http://thesis.library.caltech.edu/5058/>.
- Hough, B.G., Fan, M., Passey, B.H., 2014. Calibration of the clumped isotope geothermometer in soil carbonate in Wyoming and Nebraska, USA: implications for paleoelevation and paleoclimate reconstruction. *Earth Planet. Sci. Lett.* 391, 110–120. <http://dx.doi.org/10.1016/j.epsl.2014.01.008>.
- Huntington, K.W., Eiler, J.M., Affek, H.P., Guo, W., Bonifacie, M., Yeung, L.Y., Came, R., 2009. Methods and limitations of “clumped” CO_2 isotope (Δ_{47}) analysis by gas-source isotope ratiomass spectrometry. *J. Mass Spectrom.* 44, 1318–1329. <http://dx.doi.org/10.1002/jms.1614>.
- Hyland, E., Sheldon, N.D., Van der Voo, R., Badgley, C., Abravitch, A., 2015. A new paleoprecipitation proxy based on soil magnetic properties: implications for expanding paleoclimate reconstructions. *Geol. Soc. Am. Bull.*, 1–7. <http://dx.doi.org/10.1130/B31207.1>.
- Kaiser, J., Schefus, E., Lamy, F., Mohtadi, M., Hebbeln, D., 2008. Glacial to Holocene changes in sea surface temperature and coastal vegetation in north central Chile: high versus low latitude forcing. *Quat. Sci. Rev.* 27 (21–22), 2064–2075. <http://dx.doi.org/10.1016/j.quascirev.2008.08.025>.
- Kim, S.-T., O’Neil, J.R., 1997. Equilibrium and nonequilibrium oxygen isotope effects in synthetic carbonates. *Geochim. Cosmochim. Acta* 61 (16), 3461–3475. [http://dx.doi.org/10.1016/S0016-7037\(97\)00169-5](http://dx.doi.org/10.1016/S0016-7037(97)00169-5).
- Kluge, T., Affek, H.P., Zhang, Y.G., Dublyansky, Y., Spötl, C., Immenhauser, A., Richter, D.K., 2014. Clumped isotope thermometry of cryogenic cave carbonates. *Geochim. Cosmochim. Acta* 126, 541–554. <http://dx.doi.org/10.1016/j.gca.2013.11.011>.
- Kluge, T., John, C.M., Jourdan, A.-L., Davis, S., Crawshaw, J., 2015. Laboratory calibration of the calcium carbonate clumped isotope thermometer in the 25–250°C temperature range. *Geochim. Cosmochim. Acta* 157, 213–227. <http://dx.doi.org/10.1016/j.gca.2015.02.028>.
- Kohn, M.J., 2010. Carbon isotope compositions of terrestrial C3 plants as indicators of (paleo)ecology and (paleo)climate. *Proc. Natl. Acad. Sci. USA* 107 (46), 19691–19695. <http://dx.doi.org/10.1073/pnas.1004933107>.
- Kull, C., Grosjean, M., Veit, H., 2002. Modeling modern and Late Pleistocene glacio-climatological conditions in the north Chilean Andes (29–30°S). *Clim. Change* 52, 359–381.
- Lacelle, D., 2007. Environmental setting, (micro)morphologies and stable C-O isotope composition of cold climate carbonate precipitates—a review and evaluation of their potential as paleoclimatic proxies. *Quat. Sci. Rev.* 26 (11–12), 1670–1689. <http://dx.doi.org/10.1016/j.quascirev.2007.03.011>.
- Lamy, F., Hebbeln, D., Wefer, G., 1999. High-resolution marine record of climatic change in mid-latitude Chile during the last 28,000 years based on terrigenous sediment parameters. *Quat. Res.* 51, 83–93. <http://dx.doi.org/10.1006/qres.1998.2010>.
- Landi, A., Mermut, A., Anderson, D., 2003. Origin and rate of pedogenic carbonate accumulation in Saskatchewan soils, Canada. *Geoderma* 117 (1–2), 143–156. [http://dx.doi.org/10.1016/S0016-7061\(03\)00161-7](http://dx.doi.org/10.1016/S0016-7061(03)00161-7).
- Lechler, A.R., Niemi, N.A., 2011. The influence of snow sublimation on the isotopic composition of spring and surface waters in the southwestern United States: implications for stable isotope-based paleoaltimetry and hydrologic studies. *Bull. Geol. Soc. Am.* 124 (3–4), 318–334. <http://dx.doi.org/10.1130/B30467.1>.
- Leier, A., McQuarrie, N., Garzione, C., Eiler, J., 2013. Stable isotope evidence for multiple pulses of rapid surface uplift in the central Andes, Bolivia. *Earth Planet. Sci. Lett.* 371–372, 49–58. <http://dx.doi.org/10.1016/j.epsl.2013.04.025>.
- Liu, B., Phillips, F., Campbell, A., 1996. Stable carbon and oxygen isotopes of pedogenic carbonates, Ajo Mountains, southern Arizona: implications for paleoenvironmental change. *Palaeogeogr. Palaeoclimatol. Palaeoecol.* 124, 233–246.
- Machette, M.N., 1985. Calcic soils of the southwestern United States. *Spec. Pap. Geol. Soc. Am.* 203, 1–22.
- Mack, G.H., James, W.C., Monger, H.C., 1993. Classification of paleosols. *Geol. Soc. Am. Bull.* 105 (2), 129–136. [http://dx.doi.org/10.1130/0016-7606\(1993\)105<0129:COP>2.3.CO;2](http://dx.doi.org/10.1130/0016-7606(1993)105<0129:COP>2.3.CO;2).
- Martícorena, C., Squeo, F.A., Arancio, G., 2001. Catálogo de la Flora Vascular de la IV Región de Coquimbo. In: Squeo, F.A., Arancio, G., Gutiérrez, J.R. (Eds.), *Libro Rojo de la Flora Nativa y de los Sitios Prioritarios para su Conservación: Región de Coquimbo*. Ediciones Universidad de La Serena, La Serena, pp. 105–142.
- Meyer, N.A., Breecker, D.O., Young, M.H., Litvak, M.E., 2014. Simulating the effect of vegetation in formation of pedogenic carbonate. *Soil Sci. Soc. Am. J.* 78 (3), 914–924. <http://dx.doi.org/10.2136/sssaj2013.08.0326>.
- Monger, H.C., Wilding, L.P., 2006. Inorganic carbon: composition and formation. In: Lal, R. (Ed.), *Encyclopedia of Soil Science*, 2nd ed. Taylor & Francis, New York, pp. 886–889.
- Nordt, L.C., Driese, S.D., 2010. New weathering index improves paleorainfall estimates from Vertisols. *Geology* 38, 407–410. <http://dx.doi.org/10.1130/G30689.1>.
- Passey, B.H., Levin, N.E., Cerling, T.E., Brown, F.H., Eiler, J.M., 2010. High-temperature environments of human evolution in East Africa based on bond ordering in paleosol carbonates. *Proc. Natl. Acad. Sci. USA* 107 (25), 11245–11249. <http://dx.doi.org/10.1073/pnas.1001824107>.
- Peters, N.A., Huntington, K.W., Hoke, G.D., 2013. Hot or not? Impact of seasonally variable soil carbonate formation on paleotemperature and O-isotope records from clumped isotope thermometry. *Earth Planet. Sci. Lett.* 361, 208–218. <http://dx.doi.org/10.1016/j.epsl.2012.10.024>.
- Quade, J., Breecker, D.O., Daeron, M., Eiler, J., 2011. The paleoaltimetry of Tibet: an isotopic perspective. *Am. J. Sci.* 311 (2), 77–115. <http://dx.doi.org/10.2475/02.2011.01>.
- Quade, J., Eiler, J., Daeron, M., Achyuthan, H., 2013. The clumped isotope geothermometer in soil and paleosol carbonate. *Geochim. Cosmochim. Acta* 105, 92–107. <http://dx.doi.org/10.1016/j.gca.2012.11.031>.
- Quade, J., Garzione, C., Eiler, J., 2007a. Paleoelevation reconstruction using pedogenic carbonates. *Rev. Mineral. Geochem.* 66 (1), 53–87. <http://dx.doi.org/10.2138/rmg.2007.66.3>.
- Quade, J., Rech, J.A., Latorre, C., Betancourt, J.L., Gleeson, E., Kalin, M.T.K., 2007b. Soils at the hyperarid margin: the isotopic composition of soil carbonate from the Atacama Desert, Northern Chile. *Geochim. Cosmochim. Acta* 71, 3772–3795. <http://dx.doi.org/10.1016/j.gca.2007.02.016>.
- Retallack, G.J., 2005. Pedogenic carbonate proxies for amount and seasonality of precipitation in paleosols. *Geology* 33 (4), 333. <http://dx.doi.org/10.1130/G21263.1>.
- Ringham, M.C., Hoke, G., Huntington, K., Aranibar, J., 2016. Influence of vegetation type and site-to-site variability on soil carbonate clumped isotope records, Andean piedmont of Central Argentina (32–34°S). *Earth Planet. Sci. Lett.* 440, 1–11. <http://dx.doi.org/10.1016/j.epsl.2016.02.003>.
- Riquelme, R., Rojas, C., Aguilar, G., Flores, P., 2011. Late Pleistocene–early Holocene paraglacial and fluvial sediment history in the Turbio valley, semiarid Chilean Andes. *Quat. Res.* 75 (1), 166–175. <http://dx.doi.org/10.1016/j.yqres.2010.10.001>.
- Rodhe, A., 1998. Snowmelt-dominated systems. In: Kendall, C., McDonnell, J.J. (Eds.), *Isotope Tracers in Catchment Hydrology*. Elsevier, Amsterdam, p. 839.
- Romanek, C.S., Grossman, E.L., Morse, J.W., 1992. Carbon isotopic fractionation in synthetic aragonite and calcite: effects of temperature and precipitation rate. *Geochim. Cosmochim. Acta* 56 (1), 419–430. [http://dx.doi.org/10.1016/0016-7037\(92\)90142-6](http://dx.doi.org/10.1016/0016-7037(92)90142-6).
- Rowley, D.B., Pierrehumbert, R.T., Currie, B.S., 2001. A new approach to stable isotope-based paleoaltimetry: implications for paleoaltimetry and paleohypsometry of the High Himalaya since the Late Miocene. *Earth Planet. Sci. Lett.* 188 (1–2), 253–268. [http://dx.doi.org/10.1016/S0012-821X\(01\)00324-7](http://dx.doi.org/10.1016/S0012-821X(01)00324-7).
- Snell, K.E., Thrasher, B.L., Eiler, J.M., Koch, P.L., Sloan, L.C., Tabor, N.J., 2013. Hot summers in the Bighorn Basin during the early Paleogene. *Geology* 41 (1), 55–58. <http://dx.doi.org/10.1130/G33567.1>.
- Snell, K.E., Koch, P.L., Druschke, P., Foreman, B.Z., Eiler, J.M., 2014. High elevation of the “Nevadaplano” during the Late Cretaceous. *Earth Planet. Sci. Lett.* 386, 52–63. <http://dx.doi.org/10.1016/j.epsl.2013.10.046>.
- Stern, L.A., Baisden, W.T., Amundson, R., 1999. Processes controlling the oxygen isotope ratio of soil CO_2 : analytic and numerical modeling. *Geochim. Cosmochim. Acta* 63 (6), 799–814.
- Strauch, G., Oyarzun, J., Fiebig-Wittmaack, M., González, E., Weise, S.M., 2006. Contributions of the different water sources to the Elqui river runoff (northern Chile) evaluated by H/O isotopes. *Isot. Environ. Health Stud.* 42, 303–322. <http://dx.doi.org/10.1080/10256010600839707>.
- Suarez, M.B., Passey, B.H., Kaakinen, A., 2011. Paleosol carbonate multiple isotopologue signature of active east Asian summer monsoons during the late Miocene and Pliocene. *Geology* 39 (12), 1151–1154. <http://dx.doi.org/10.1130/G32350.1>.
- Tabor, N.J., Myers, T.S., Huffington, R.M., Sciences, E., Gulbranson, E., Rasmussen, C., Sheldon, N.D., 2013. Carbon stable isotope composition of modern calcareous soil profiles in California: implications for CO_2 reconstructions from calcareous paleosols. In: SEPM Special Publications, vol. 104, pp. 17–34.
- Tobin, T.S., Schauer, A.J., Lewarch, E., 2011. Alteration of micromilled carbonate $\delta^{18}\text{O}$ during Kiel Device analysis. *Rapid Commun. Mass Spectrom.* 25 (15), 2149–2152. <http://dx.doi.org/10.1002/rcm.5093>.
- Tripathi, A.K., Hill, P.S., Eagle, R.A., Mosenfelder, J.L., Tang, J., Schauble, E.A., Eiler, J.M., Zeebe, R.E., Uchikawa, J., Coplen, T.B., Ries, J.B., Henry, D., 2015. Beyond temperature: clumped isotope signatures in dissolved inorganic carbon species and the influence of solution chemistry on carbonate mineral composition. *Geochim. Cosmochim. Acta* 166, 344–371. <http://dx.doi.org/10.1016/j.gca.2015.06.021>.
- Wang, Y., Amundson, R., Trumbore, S., 1994. A model for soil $^{14}\text{CO}_2$ and its implications for using ^{14}C to date pedogenic carbonate. *Geochim. Cosmochim. Acta* 58, 393–399. [http://dx.doi.org/10.1016/0016-7037\(94\)90472-3](http://dx.doi.org/10.1016/0016-7037(94)90472-3).
- Zaarur, S., Affek, H.P., Brandon, M.T., 2013. A revised calibration of the clumped isotope thermometer. *Earth Planet. Sci. Lett.* 382, 47–57. <http://dx.doi.org/10.1016/j.epsl.2013.07.026>.
- Zech, R., Kull, C., Veit, H., 2006. Late Quaternary glacial history in the Encierro Valley, northern Chile (29°S), deduced from ^{10}Be surface exposure dating. *Palaeogeogr. Palaeoclimatol. Palaeoecol.* 234, 277–286. <http://dx.doi.org/10.1016/j.palaeo.2005.10.011>.